ground water

On the Relation Between Steep Monoclinal Flexure Zones and Steep Hydraulic Gradients

by Y. Yechieli[1], U. Kafri[2], S. Wollman[2], V. Lyakhovsky[2], and R. Weinberger[2]

Abstract

Steep hydraulic gradients are found in association with steep monoclinal flexures. However, the physics of the reduction of the hydraulic conductivity, which is responsible for the steep gradients, has seldom been studied. We present results of hydrological and mechanical modeling aiming to study the effect of such steep hydraulic gradients demonstrated in the Judea Group Aquifer system, Israel. The hydrological configuration of steep dips and anisotropy between flows parallel and perpendicular to the bedding planes was simulated using the FEFLOW code. It exhibited a situation whereby part of the flow is oblique to the bedding planes and therefore some steepening of the hydraulic gradients occurred due to actual conductivity reduction. However, this reduction is not enough to account for the steeper gradients observed. The effect of a deep-seated reverse fault under the monocline on the permeability distribution within the structure was examined by numerical mechanical simulations. It exhibited a compressional stress distribution in the steep part of the monocline, which, due to shortening and closure of joints and voids, is presumably responsible for a significant pressure-induced permeability reduction. This process by itself in a layered structure, including interlayering of thin marl layers, could be responsible for the steep hydraulic gradients in the steep part of the monocline.

Introduction

Steep hydraulic gradients are known from many hydrological systems around the world. These gradients are best explained by low hydraulic conductivity, owing to fault zones, tight folds, lateral sedimentological facies variations, and other geological barriers (e.g., Fridrich et al. 1994; Wirt and Hjalmarson 1999). Such zones are usually limited in extent, and data regarding the hydrological regimes are scarce. However, several studies conducted in the vicinity of faults show a significant reduction in hydraulic conductivity associated with them (e.g., Yechieli et al. 2001; Bense et al. 2003; Seaton and Burbey 2005). Other studies have shown the effect of fracture zones on the hydrological regime (e.g., Forster and Smith 1988). Sibson (1996) showed how different combinations of hydraulic gradients, intrinsic permeability, anisotropy, and structural position lead to complex three-dimensional flow paths. The variations in the hydraulic conductivity across folds and monoclines have seldom been studied.

The objective of this study was to explore the hydrological regime across a steep monoclinal flexure zone and to analyze the variations in hydraulic gradients perpendicular to the structure. We focus on the Ramallah monocline, which is one of tens of folds and monoclines comprising the approximately 1000-km-long fold belt known as the "Syrian Arc" system (Krenkel 1924). A generalized cross section (Figures 1A and 1B) exhibits the structural and the hydrogeological configuration of the study area. The present study focuses on the interrelationship between the steep limb of the Ramallah monocline (termed hereafter "monoclinal flexure zone") and the coincident steep ground water hydraulic gradients across this zone. The latter require, from the hydrological point of view, a reduction of hydraulic conductivity in this segment of the flow system. We analyzed the structural configuration and mechanism that might be responsible for this reduction of permeability and thus of the hydraulic conductivity. We show that oblique flow to the bedding planes and pressure-induced permeability reduction

[1]Corresponding author: Geological Survey of Israel, Jerusalem 95501, Israel; vladi@gsi.gov.il

[2]Geological Survey of Israel, Jerusalem 95501, Israel.

Received August 2006, accepted February 2007.

doi: 10.1111/j.1745-6584.2007.00327.x

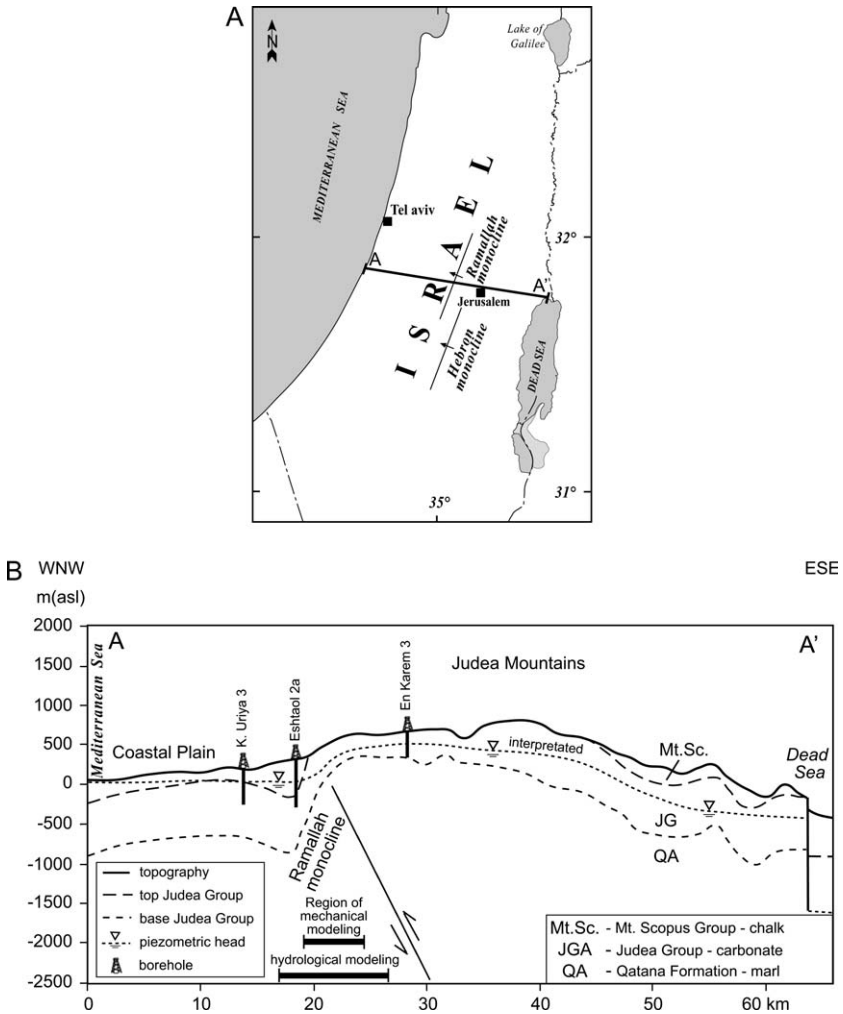

Figure 1. (A) Location map of Ramallah and Hebron monoclines; arrows point to the steep flank of the monoclines. (B) Hydrogeological cross section (A–A′) from the Mediterranean Sea to the Dead Sea.

in the flexure zone are responsible for the steep gradients across the monocline.

Hydrogeological Background

The Cretaceous carbonate Judea Group Aquifer (JGA) is one of the main water sources in Israel. The aquifer is bounded at its base by confining marl layers of Qatana Formation of Lower Cretaceous age and at its top, in some areas, by the confining chalk and marl layers of the Upper Cretaceous Mt. Scopus Group. A detailed lithostratigraphic description of the Judea Group was given by Arkin et al. (1965) and Arkin and Hamaoui (1967). In the Judea Mountains, this sedimentary sequence constitutes an anticlinorium and a hydrological divide between the Mediterranean and the Dead Sea (Figure 1).

The JGA is composed mainly of limestone and dolomite beds. The sequence also contains marl beds with thicknesses varying from a few centimeters to several meters. Karstic phenomena such as caves, solution channels, and open cracks are more abundant in the upper part of the JGA. The JGA has been subdivided hydrologically into lower and upper subaquifers (Guttman 1980). These two, in spite of an apparent difference in their hydraulic properties, are probably interconnected, feeding each other and acting as one hydrological unit. In parts of the monoclinal segment of the ground water system and east of it, the upper JGA comprises a vadose zone that feeds the saturated lower JGA (Figure 1). Only in the western part of the aquifer is the entire sequence of the JGA saturated, acting as one connected hydrological unit. Hence, the aquifer is unconfined in some areas and confined in others.

Structural Background

The general structural framework is evident in the top-Judea Group structural map of Fleischer and Gafsou (2000). The anticlinorium and its subsidiary folds are part of the Syrian Arc system (Krenkel 1924). The system in Israel consists of north-east-trending synclines and monoclines that overlie deep-seated reverse faults. These structures were discussed by De Sitter (1962), Freund (1965), Mimran (1976), and Reches et al. (1981), among others. The following are the characteristics of the Ramallah and Hebron monoclines (Reches et al. 1981):

1. Dips are steep and variable, attaining maximum values of 50° westward.
2. The monoclines are underlain by a deep-seated reverse fault that dips approximately 70° eastward. The inferred total throw along the fault at a depth of 4 km is 1.2 km.
3. An analysis of small-scale structures reveals areas of both shortening and extension. The monoclinal flexure zone is characterized by small structures such as tectonic stylolites and small reverse faults that commonly exhibit shortening perpendicular to the monocline axis.

Methods

The present study included collection of hydraulic data as well as hydrologic and mechanical simulations:

1. Piezometric head data were obtained from the Hydrological Service of Israel data base and from borehole logs in the Geological Survey of Israel archives in order to construct a hydrogeological cross section and to determine hydraulic gradients. Transmissivities (T) were obtained from pumping test results and hydraulic conductivities (K) and permeabilities (k) were calculated accordingly.
2. Simulated hydraulic heads were obtained using the numerical FEFLOW code (Diersch 2005) in order to examine the effect of various hydrologic factors such as permeability, anisotropy, and flexure angle.
3. Stress distribution within the monocline was simulated in order to study the possible effect of rock deformation on hydraulic conductivity.

The paper is organized in two main parts, including the hydrological and mechanical simulations. In each part, the methodology is explained together with the results and discussion of these specific topics.

Results and Discussion

Piezometric Heads and Hydraulic Gradients

Piezometric head data along the studied cross section are sparse and not synchronous. Nevertheless, a general configuration could be obtained using the best available data. The hydraulic gradient basically reflects the geological structure (Figure 1B). In the central recharge area, in the vicinity of Jerusalem, the layers are subhorizontal and the hydraulic gradient is small, around 2×10^{-4}. Water levels are between 450 and 480 m above sea level, and the hydrological divide occurs near the En Karem 3 borehole. The ground water level in Eshtaol 2a, to the west, is 17 m above sea level. The calculated hydraulic gradient between the two boreholes is steep, around 5×10^{-2}. The hydraulic gradient in the monoclinal flexure zone itself is expected to be steeper, but there are no direct data to support this assumption.

From the foothills region westward through the coastal plain, the hydraulic gradient is again small, less than 1×10^{-3}. Thus, the hydraulic gradient in the monoclinal flexure zone of the system is steeper by more than an order of magnitude than those east and west of this zone. This analysis suggests reduced conductivities in the flexure zone as compared to adjacent segments.

Hydrological Properties

Hydrological properties of the JGA obtained from pumping tests in the study area (i.e., transmissivities and calculated conductivities) are sparse. In the eastern part of the monocline, transmissivities (T) and conductivities (K) are relatively low. Values of T vary between 10^0 and 10^3 m^2/d and are mostly about 10^2 m^2/d. The corresponding K values are mostly around 1 m/d. The area to the west of the monocline exhibits considerably higher T and K values. T values are mostly between 10^3 and 10^4 m^2/d and K values between 10^1 and 10^2 m/d. From the monoclinal flexure zone, there are no hydraulic data due to lack of pumping wells drilled in the highly inclined beds. The scarcity of the data hence calls for using hydrological simulations for estimating the integrated conductivity of this zone.

Numerical Hydrological Simulations

Measured piezometric heads along the Mediterranean Sea–Dead Sea cross section exhibit, as noted previously, a very steep hydraulic gradient in the Ramallah monocline with a drop of 460 m over a distance of 10 km (average gradient of ~5×10^{-2}). One of the hypotheses to be tested was that this steep hydraulic gradient is the combined result of the highly inclined beds in the monoclinal flexure zone coupled with a high anisotropy of hydraulic conductivity whose maximum is parallel to the bedding. The dip of the bedding planes within this zone is hereafter termed the "flexure angle."

In order to test this hypothesis, we varied the flexure angle, anisotropy, and hydraulic conductivity in a model of a two-dimensional (2D) cross section using the FEFLOW code (Figure 2). The flexure angle was specified in the model by the angle of maximum hydraulic conductivity parallel to the bedding planes. The anisotropy was simulated by specifying the ratio of the hydraulic conductivity perpendicular to the bedding planes to the hydraulic conductivity parallel to the bedding planes.

Two sets of hydraulic conductivities were used in the hypothetical cross section. The first set consisted of a "uniform" conductivity ($K = 1$ m/d) for the entire cross section in order to test the effect of the flexure angle and that of the anisotropy separately. The other set consisted of three segments of hydraulic conductivity representing approximate "actual" field values of the cross section, as shown in Figure 2: the zone west of the monocline was assigned 10 m/d, the monoclinal flexure zone itself was assigned 0.1 m/d. and the eastern limb of the monocline was assigned 1 m/d. A very low hydraulic conductivity of $K = 0.001$ m/d was assigned to the Upper Cretaceous aquitard overlying the JGA west of the monocline.

Two flexure angles were chosen, 18° and 30°, representing the dips observed along the monoclinal flexure zone. In addition to a case of an isotropic media and in order to examine the effect of anisotropy, a relatively high value of anisotropy (10^{-2}) was applied. This value is an order of magnitude higher than that used in previous studies (Mancy et al. 2000; Flexer et al. 2003).

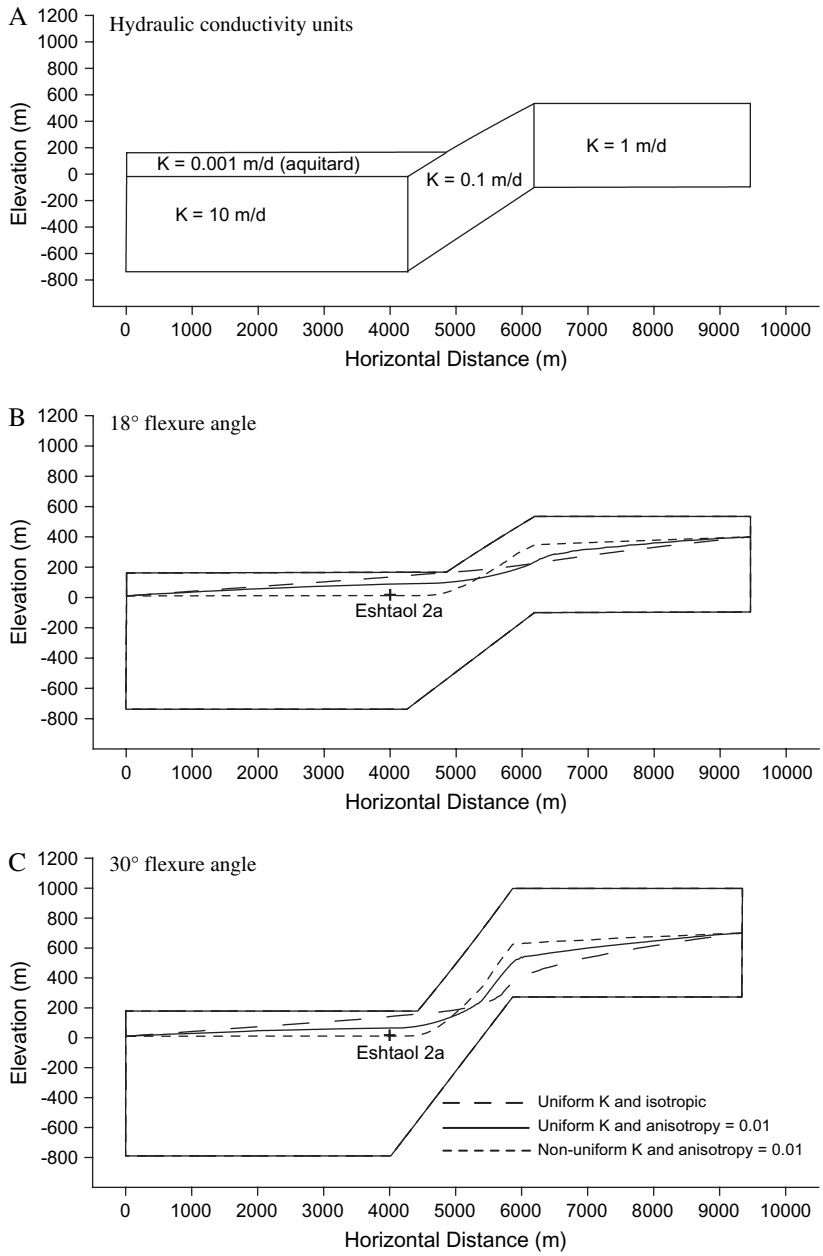

Figure 2. (A) Hydraulic conductivity values of the different subzones, for the nonuniform case. For the uniform case, the value of $K = 1$ m/d is used for all subzones, except for the overlying aquitard, (B) simulated piezometric heads at an 18° flexure angle for various hydraulic conductivities and anisotropy ratios, (C) simulated piezometric heads at a 30° flexure angle. Note that in the simulation of 30°, a somewhat steeper hydraulic gradient is obtained even for an isotropic situation. This may be partly explained by the apparent reduction in the flow section in this unrealistic isotropic situation.

The boundary conditions of the model were set as follows: The western boundary consisted of a fixed head set at 10 m above sea level, corresponding to actual piezometric head data in the western part of the JGA close to the Mediterranean Sea. The eastern boundary was set at a fixed head of 400 m above sea level for the 18° flexure angle, corresponding to actual piezometric head data in the eastern part of the JGA. For the 30° flexure angle, the eastern boundary was set at a hypothetical fixed head of 700 m above sea level. This higher hypothetical fixed head was used for geometrical reasons only, even though it is higher than the actual measured heads. No recharge was assigned from the top since the actual area of the monocline is small and the recharge was expected to be insignificant. The simulations were performed for steady-state conditions.

Hydrological Simulations

The results of the simulations are shown in Figures 2 and 3 for the different scenarios of flexure angles, degree of anisotropy, and nonuniformity in hydraulic conductivity. These figures demonstrate hydraulic gradients and flow pathlines for various cases. The simulations show that the anisotropy has some effect on the hydraulic gradient (Figure 2). The hydraulic gradient in the monoclinal flexure zone is steeper in the case of high anisotropy than in the case of isotropic media. The steepening of the hydraulic gradient for the anisotropic case is expected

since some of the water flows oblique to the bedding planes and not parallel to bedding along the maximum conductivity (Figure 3). However, the relatively high anisotropy and the flexure angle alone do not account for the actual steep hydraulic gradient encountered in the Ramallah monocline. Hence, the next set of simulations was conducted for the case of nonuniform distribution of hydraulic conductivity, in which a lower conductivity was assigned to the monoclinal flexure zone. These simulations yielded a significant increase in the hydraulic gradient, as observed in the field (Figure 2). The simulated piezometric heads at Eshtaol 2a borehole is in good agreement with the observed head of 17 m above sea level for the nonuniform high-anisotropy case (Figure 2B). The extrapolated simulated piezometric head at the location of En Karem 3, which is outside of the model boundary, is also in good agreement with the observed head of 480 m above sea level. Subsequently, mechanical simulations were run in order to understand the reasons for the lower conductivity in the monocline.

Mechanical Simulations of Stress Distribution during Monocline Formation

Stress-Permeability Relation

Stress affects rock permeability by opening or closing preexisting microcracks and pores, changing microcrack

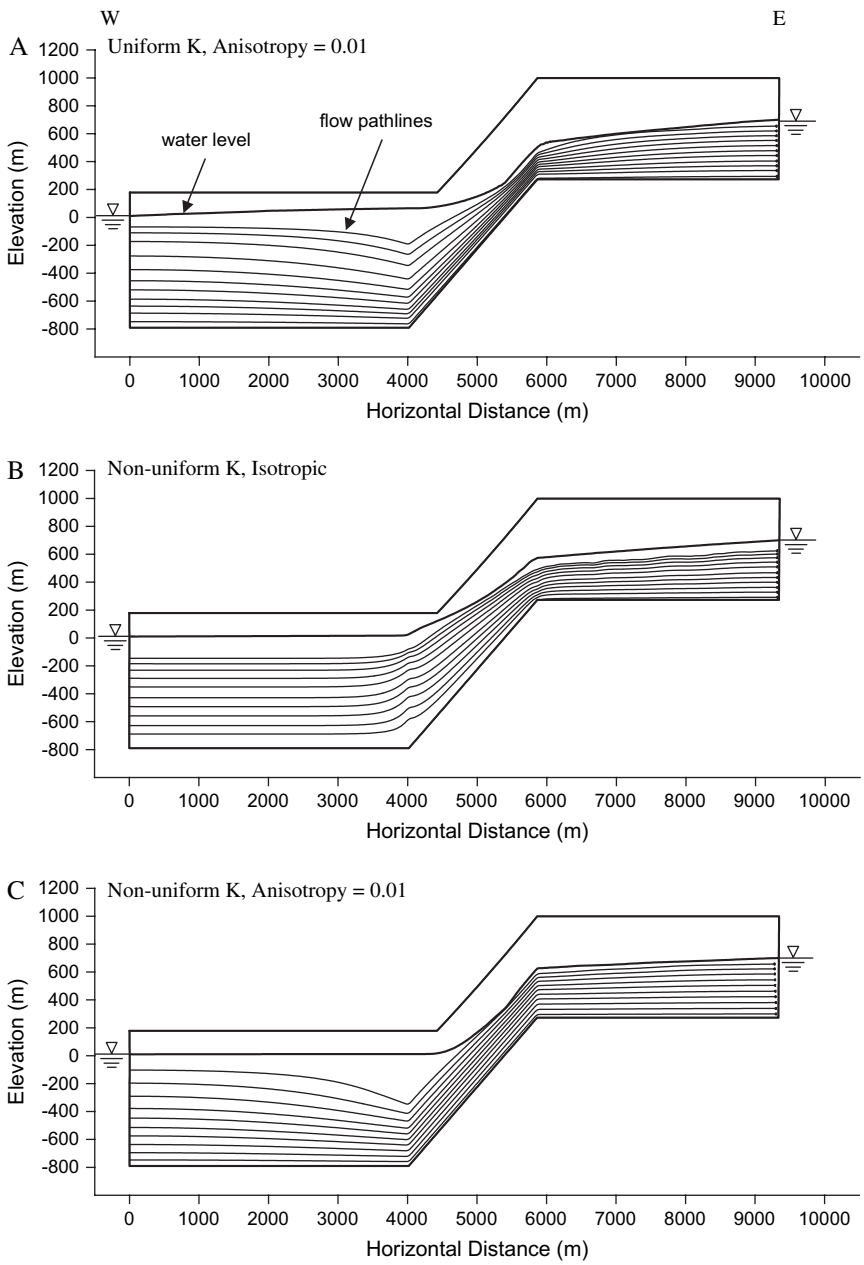

Figure 3. Simulations of flow pathlines and piezometric heads for a 30° flexure angle for the following scenarios: (A) uniform *K*, an anisotropy of 10^{-2} showing some steepening of the hydraulic gradient, probably due to the partial water flow oblique to the bedding planes, (B) hypothetically isotropic and nonuniform *K* showing a somewhat steeper hydraulic gradient, (C) nonuniform *K* and anisotropy where a considerable steepening of the hydraulic gradient is observed, similar to the actual observed values.

apertures, and through increase of the rock fracturing. In studying the stress in the crust, it is convenient to subtract the mean stress $\sigma_m = (\sigma_{11} + \sigma_{22} + \sigma_{33})/3$ from the normal stress components σ_{ij} ($i, j = 1, 2, 3$). The mean stress is termed also in the rock mechanics literature as confining pressure P_c, where the compressive stress reckons positive. Accordingly, the deviatoric stress is defined as a tensor $\tau_{ij} = \sigma_{ij} - \sigma_m\delta_{ij}$, where δ_{ij} is the unit tensor. The deviatoric stress mostly controls the intensity of the fracturing process that can be estimated through calculating the Coulomb failure stress (CFS) (e.g., Jaeger and Cook 1969). Observations in laboratory rock experiments and in the earth crust also underscore the interaction between deviatoric stress and pore pressure in porous rocks (e.g., Skempton 1954; Wang 1997; Ge and Stover 2000; Lockner and Stanchits 2002). Rock dilation and related pore pressure reduction have long been recognized (e.g., Paterson 1978) and recently confirmed in accurate laboratory experiments (Hart and Wang 1999; Lockner and Stanchits 2002). This interaction has been approached by incorporating the constitutive relations of anisotropic (Biot and Willis 1957) or nonlinear (Hamiel et al. 2005) porous media. While the dilatancy of porous rocks has a pronounced effect on the pressure change (Wang 1997; Ge and Stover 2000; Hamiel et al. 2005), still the pressure is the major factor controlling the permeability change. Relationships between the rock permeability and the pressure have been evaluated for fractured rocks based upon asperity deformation models of rough cracks and the cubic relation between flow rate and aperture (e.g., Gangi 1978; Walsh and Grosenbaugh 1979; Walsh 1981; Walsh and Brace 1984). Using an exponential size distribution of asperities, Walsh (1981) found the permeability to vary as:

$$\left(\frac{\kappa}{\kappa_0}\right)^{\frac{1}{3}} = 1 - \sqrt{2}\frac{h}{a_0}\ln\left(\frac{P_e}{P_{e0}}\right) \tag{1}$$

where κ is permeability, κ_0 is the permeability at a reference effective pressure P_{e0}, h is the root mean square height distribution of the asperities in the fracture, a_0 is the aperture half width at some reference pressure P_{e0}, and P_e is the actual effective pressure. Following the notation accepted in rock mechanics literature (e.g., Lockner and Stanchits 2002), we define the effective pressure as a difference between the mean stress or confining pressure and the fluid pressure P_f:

$$P_e = P_c - P_f \tag{2}$$

The variation in the permeability with the effective pressure calculated with Equation 1 has successfully matched experimental data for fractured rocks (e.g., Walsh 1981; Walsh and Brace 1984; Raven and Gale 1985; Morrow et al. 1986) and shale (Kwon et al. 2001). Even stronger decrease in permeability was predicted by Germanovich and Astakhov (2004), who consider crack interaction in a model with closely spaced joints.

The permeability of rocks may be significantly enhanced if the CFS (e.g., Jaeger and Cook 1969),

$$\mathrm{CFS} = \tau - \mu P_e - S, \tag{3}$$

is high enough to increase rock fracturing. This fracturing may occur under high values of the deviatoric stress relative to the effective pressure, where $\tau^2 = \tau_{ij}\tau_{ij}/2$ (Einstein's summation convention is assumed), S is the cohesion, and μ is the coefficient of internal friction. The calculation of the CFS is one of the most widely used criteria to characterize the conditions under which rock failure occurs (e.g., Jaeger and Cook 1969). The advantage of this calculation to predict rock failure has been supported by laboratory rock experiments as well as by reasonable agreement between regions of predicted increase of coseismic Coulomb stress and the location of aftershocks (e.g., Harris 1998). The mapping of the CFS distribution enables localizing high-fracture zones that can serve as either conduits or barriers for fluid flow, depending on crack orientations controlled by the principal stress directions.

Model Setup

A series of 2D simulations were performed to analyze the stress distribution associated with formation of a monocline above a deep-seated reverse fault dipping approximately 70° eastward. The initial geometry of the model reflects the original horizontal sedimentary layers prior to the formation of the fault. A numerical code based on Fast Lagrangian Analyses of Continua algorithm (Poliakov et al. 1993) was employed to examine stress distribution in a 2D plane-strain solution for Maxwell visco-elastic media. A similar algorithm was adopted by Maimon et al. (2005) for simulating stress distribution in a media governed by the Drucker-Prager plasticity model (e.g., Hill 1998). For simplicity, the stress simulation was not fully coupled with the ground water flow model. The evolution of effective pressure was calculated assuming that fluid pressure is always hydrostatic. The stress distribution was simulated in a rectangular area of 4 by 0.8 km, divided into several layers according to a schematic representation of the Judea Group sequence and the overlying chalk layers of the Mount Scopus Group (Figure 4). Most of the section consists of the relatively stiff dolomite layers of the Judea Group (material unit #1 in Figure 4) separated into five sublayers by thin and weak marl layers (material unit #2). The upper part of the stack of layers consists of a chalk layer (material unit #3), and the lower part of the section is an alternating sequence of limestone and marl (material unit #4). The mechanical properties assigned to these material units in the mechanical simulations are based on available rock mechanics experiments and in situ measurements. Hatzor and Palchik (1997) and Palchik and Hatzor (2000) investigated the relation between porosity, grain size, microstructure, and mechanical properties for dolomites of the Judea Group (material unit #1) and found an average Young's modulus $E = 3 \times 10^{10}$ Pa. The Young's modulus of limestone is slightly lower than that of dolomite. The base of the simulated stack of layers is characterized by alternating limestone and marl. The mechanical properties have not been measured either in situ or in the laboratory. Since the marl

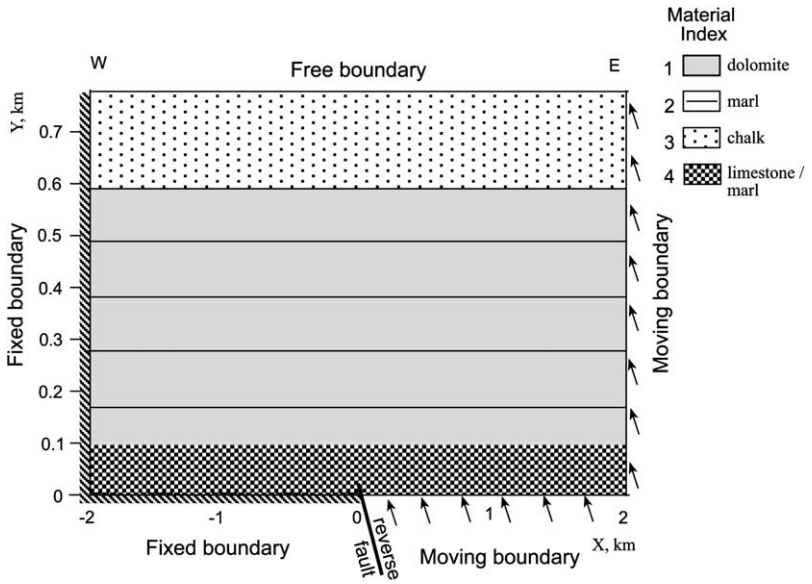

Figure 4. Schematic model setup used in the mechanical simulations, showing the structure of the simulated area and the boundary conditions.

significantly reduces the overall stiffness of the composite lithology, a value of $E = 3 \times 10^9$ Pa was assigned to that unit.

The Young's modulus of chalk (material unit #3) is equal to $E = 3 \times 10^9$ Pa (Hatzor et al. 2002). Marl (material unit #2) is softer than chalk, with an in situ Young's modulus between 3×10^8 and 3×10^9 Pa (Aisenstein et al. 1966). An intermediate value of $E = 10^9$ Pa was used in the simulations. In contrast to the brittle behavior of dolomite and chalk, the rheological behavior of the marl under low-strain rates of a monocline formation is not clear. It may be expressed using an elasto-plastic or visco-elastic constitutive relation or both. A more general problem of the most suitable rheological behavior of weak sedimentary rocks has been extensively discussed in context of salt diapirism. Starting with the pioneering study by Ramberg (e.g., Ramberg 1981), several authors applied linear or power-law viscosity (see also Turcotte and Schubert 1982). Viscous-like deformation of sedimentary rocks was doubted by several authors (e.g., Vendeville and Jackson 1992; Weijermars et al. 1993; Vendeville 2002), who pointed out the importance of faulting processes and applied elasto-plastic rheology. Poliakov et al. (1996) were the first to combine brittle faulting and viscous flow simultaneously. They also demonstrated that the choice of the most appropriate rheology depends on the Deborah number, which is defined as the ratio of a stress relaxation time, characterizing the intrinsic fluidity of a material, and the characteristic time scale of an external load. The smaller the Deborah number is, the more fluid the material appears to be. The problem of the modeling presented is that there is no strong constraint for the relaxation time or the intrinsic fluidity of the marl; therefore, we ran two different model setups. In the first model, ductile behavior of the marl was simulated using a Maxwell visco-elastic rheology with viscosity $\eta = 10^{20}$ Pa s corresponding to relatively low Deborian numbers (De $< 10^{-2}$). In the second model, Drucker-Prager elasto-plastic rheology with an internal friction coefficient equal to 0.6 and negligible cohesion was applied. The results (see subsequently) indicate that the stress pattern is controlled by the layered structure and is not strongly sensitive to the applied rheological model. Hence, we present the results only of the second model in the following section. The model boundary conditions reproduce the relative block motion above the deep-seated reverse fault (Figure 4). The eastern boundary (right side of the simulated area) and the eastern part of the bottom move upward along the fault plane, representing the motion of the hanging wall. The western boundary (left side of the simulated area) and the western part of the bottom are fixed, representing the footwall. The upper boundary is free. We simulated the effects of folding a stack of layers with different mechanical properties on stress distribution and compared it to that of folding a homogeneous elastic layer with dolomitic properties. In both simulations, the initial stress distribution was set equal to the lithostatic pressure and was modified in accordance with the boundary displacements due to the motion.

Results and Discussion of the Mechanical Simulations

The results of the simulations are presented in Figures 5 and 6. The displacement along the reverse fault has to be about an order of magnitude higher for the layered model than that for the homogeneous model to achieve a similar magnitude of the ratio P_e/P_{e0} (Figures 5A and 5B) and CFS (Figures 6A and 6B). This is related to strain localization in the thin marl layers in the heterogeneous model, leading to mechanical detachment between the stiff dolomite layers and prohibiting upward stress transfer.

The ratio P_e/P_{e0} presented in Figure 5 could be converted to permeability values using Equation 1 for known crack geometry. In the series of experiments presented by

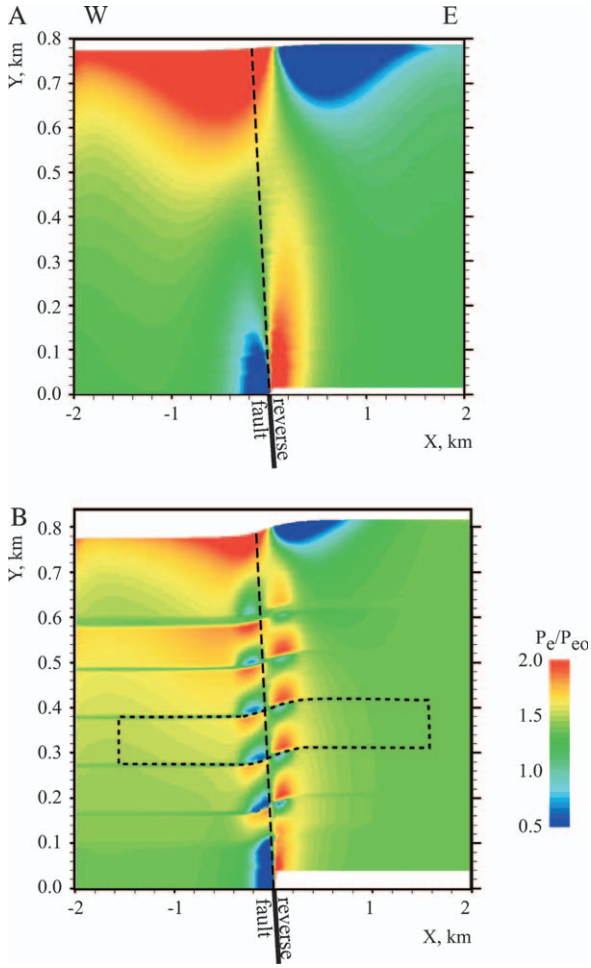

Figure 5. The ratio between the initial lithostatic pressure and pressure associated with the formation for (A) a homogeneous model and (B) a layered model. The dashed line shows the extension of the fault trace. Also shown is the 100-m-thick layer that its permeability distribution was inserted into the hydrological simulation in Figure 7.

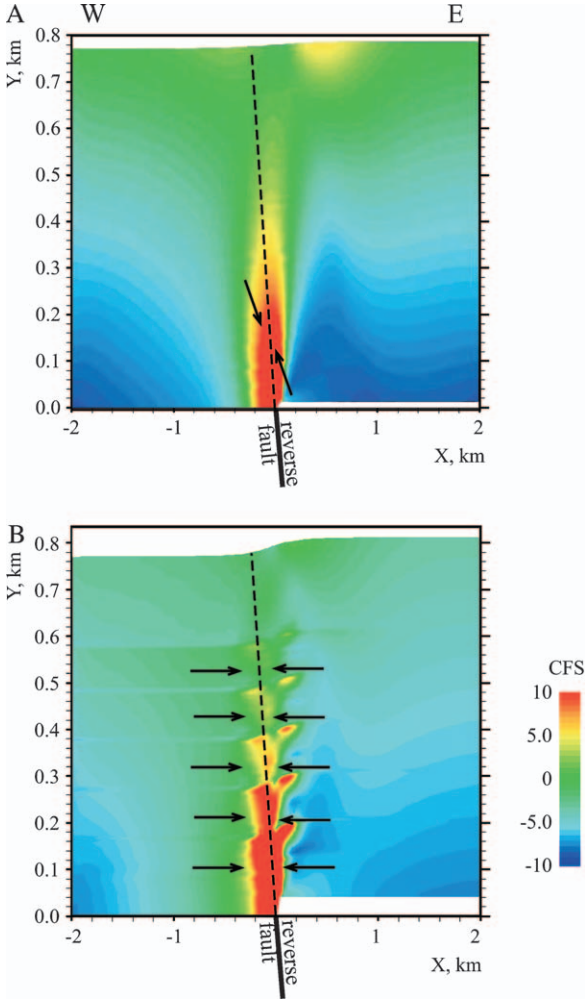

Figure 6. Distribution of CFS for (A) a homogeneous model and (B) a layered model. Arrows show the direction of maximum compressive stress. The dashed line shows the extension of the fault trace.

Walsh (1981), the value h/a_0 was estimated to be around one. This means that the permeability is very sensitive to the effective pressure. Pressure increase by a factor of 1.5 (P_e/P_{e0} ~ 1.5) may decrease the permeability up to an order of magnitude, while P_e/P_{e0} ~ 2 may decrease the permeability up to 2 orders of magnitude. In contrast to the very regular stress distribution in the homogeneous model (Figure 5A), the mechanical detachment between dolomite layers leads to the creation of several local compressive zones and almost eliminates the tensile zones (Figure 5B). The compressive zones are located at the top of each layer in the monoclinal flexure zone (west of the projected fault plane) and at the bottom of each layer east of the projected fault plane. If the permeability is reduced by an order of magnitude at these compressive zones, the overall reduction in the permeability of the aquifer explains the steep hydraulic gradients documented in the JGA.

The calculated distribution of the CFS in the homogeneous model (Figure 6A) and the orientation of the maximum compressive stress support the propagation of the deep-seated reverse fault in a direction close to its original dip. A relatively wide fracture zone with a significant fracture-enhanced permeability is expected to evolve around the fault plane. In contrast, in the layered model (Figure 6B), most of the fracturing occurs in the lowest weak layer and, as a result of mechanical detachment between the sublayers, stress is not transmitted to the upper stiff dolomite layers. Only small local regions with slightly increased CFS are recognized in the monoclinal flexure zone at the top of each sublayer. These local regions are under horizontal compression and are affected by increased pressure (Figure 5B). Therefore, if fracturing occurs in these regions, the permeability is not expected to increase but may even decrease due to pressure-induced compaction.

Several kinematic and mechanical models for fault-related folds have been proposed. Some of them explain the development of hanging-wall anticlines (e.g., Suppe 1983, 1985; Salvini et al. 2001). Other models explain both the development of footwall synclines and hanging-wall anticlines, such as trishear fault-propagation folding

and forced folding models (e.g., Erslev 1991; Hardy and Ford 1997; Allmendinger 1998) or finite-element models implementing elasto-plastic and frictional rock rheology (e.g., Cardozo et al. 2003; Weismayr and Grasemann 2005). The approach taken here emphasizes the role played by the layered structure as expressed by the differences in rock properties and layer thicknesses. The tip of the fault remains stationary, while displacement continues according to the moving boundary, similar to the model of Weismayr and Grasemann (2005). The thin and weak marl layers allow detachment between thick and stiff layers and suppress stress concentration in front of the fault tip.

Hydraulic Pressure Distribution Based on Stress-Related Permeability

An attempt was made herein to demonstrate a coupling between the pressure distribution obtained from mechanical modeling (Figure 5) and the ground water flow pattern. The pressure-related permeability was calculated for the 100-m-thick layer (shown in Figure 5), using Equation 1. According to this pressure-permeability relation, the zones of reduced hydraulic conductivity (Figure 7) coincide with those of the higher pressures. Thus pressure-related hydrological "barriers" are formed. This conductivity distribution was employed in the hydrological FEFLOW model to simulate the steady-state ground water pressure distribution (Figure 7). As expected, the relatively high ground water pressure gradients occur in the monocline flexure zone where low hydraulic conductivities exist (Figure 7). These particular zones correspond to the hydrological "barriers" described previously. In general, the simulations support the suggested mechanism responsible to the reduction of the overall hydraulic conductivity in the flexure zone.

Summary and Conclusions

An attempt was made herein to understand the factors and the mechanism responsible for the steep hydraulic gradients in monoclinal flexure zones. The a priori working hypothesis, that a reduction of conductivity could stem from the steep dip of the bedding planes and/or anisotropy in hydraulic conductivity whose maximum is parallel to the bedding, was tested by numerical simulations with the FEFLOW code. Results showed that the steep dip of the bedding planes in the monocline and anisotropy have some effect on the steepness of the hydraulic gradient but cannot account for the extremely steep gradient. Therefore, a considerable additional reduction of hydraulic conductivity in the monoclinal flexure zone is required.

Mechanical simulations were performed to obtain the stress distribution within the monocline. A sequence of dolomite and limestone layers with interlayers of marl was deformed by the movement of a deep-seated reverse fault. In the monoclinal flexure zone, above the fault and adjacent to it, a compressional stress field is evident, with local tensional areas. Most of the segment is subjected to compression. This leads to void closure, reduction of permeability, and, thus, reduction in the hydraulic conductivity. Closure of voids and fractures will also limit the extent of karst features, where most ground water flows in this system.

We conclude that formation of the monocline in mechanically layered heterogeneous material leads to a reduction of the overall hydraulic conductivity in the flexure zone. This, in turn, results in steepening of the ground water hydraulic gradient. The results of these 2D simulations obviously cannot deal with the possible enhancement of conductivities in a perpendicular direction, as discussed by Sibson (1996).

Acknowledgments

We thank Steven Ingebritsen, Alicia Wilson, and two anonymous reviewers for their constructive comments and the Hydrological Service of Israel for supplying hydrological data. This study was supported by a grant from the Israel Science Foundation—ISF 479/03.

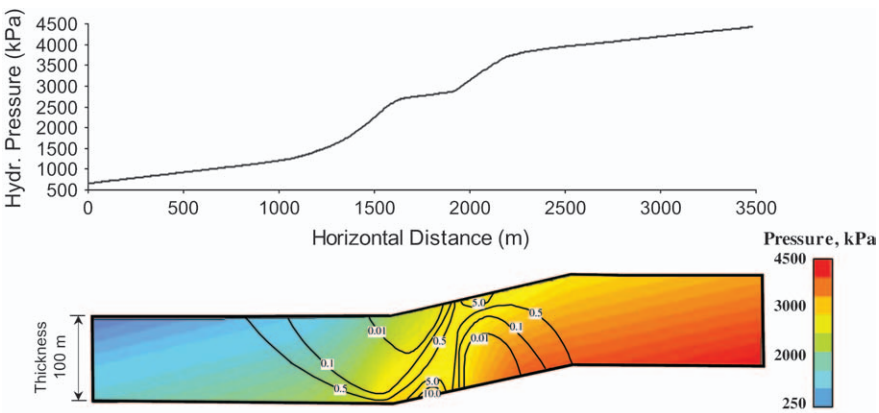

Figure 7. Simulated steady-state ground water pressure distribution as a result of hydraulic conductivity distribution, obtained from the mechanical model. Contours exhibit hydraulic conductivity values in m/d. The piezometric head difference between the inflow and outflow boundary is 400 m. The configuration of the layer used in this model was taken from Figure 5.

References

Aisenstein, B., D. David, and G. Wiseman. 1966. Mechanical properties of some marls from Israel. In *Proceedings of the First Congress International Society Rock Mechanics*, 393–397. Lisbon, Portugal.

Allmendinger, R.W. 1998. Inverse and forward numerical modeling of trishear fault-propagation folds. *Tectonics* 17, no. 4: 640–656.

Arkin, Y., and M. Hamaoui. 1967. The Judea Group (Upper Cretaceous in central and southern Israel. *Bulletin of the Geological Survey of Israel* 42. Jerusalem: Israel Geological Survey.

Arkin, Y., M. Braun, A. Starinsky, M. Hamaoui, and M. Raab. 1965. Type sections of Cretaceous formations in the Jerusalem-Bet Shemesh area. Israel Geological Survey Report. Jerusalem: Israel Geological Survey.

Bense, V.F., R.T. van Balen, and J.J. de Vries. 2003. The impact of faults on the hydrogeological conditions in the Roer Valley rift system: An overview. *Netherlands Journal of Geosciences* 82, no. 1: 41–54.

Biot, M.A., and D.G. Willis. 1957. The elastic coefficients of the theory of consolidation. *Journal of Applied Mechanics, Trans. ASME* 79, 596–601.

Cardozo, N., K. Bhalla, A.T. Zehnder, and R.W. Allmendinger. 2003. Mechanical models of fault propagation folds and comparison to the trishear kinematic model. *Journal of Structural Geology* 25, no. 1: 1–18.

De Sitter, L.U. 1962. Structural and development of the Arabian shield in Palestine. *Geologie in Aijnbouw* 41, no. 3: 116–124.

Diersch, H.-J. 2005. *Finite Element Subsurface Flow and Transport Simulation System, User's Manual, FEFLOW Version 5.2*. Berlin, Germany: WASV GmbH.

Erslev, E.A. 1991. Trishear fault-propagation folding. *Geology* 19, no. 6: 617–620.

Fleischer, L., and R. Gafsou. 2000. Top Judea Group—Digital structural map of Israel. Phase III. Geophysical Institute of Israel Rep. 873/55/99. Lod, Central Israel: Geophysical Institute of Israel.

Flexer, A., H. Hotzl, W. Ali, J. Bensabat, J. Guttman, and A. Yellin-Dror. 2003. A 3D hydrogeological model of the Marsaba Feshchah region. Final report. Project no. WT004. Tel-Aviv, Israel.

Forster, C., and L. Smith. 1988. Groundwater flow systems in mountainous terrain, 2. Controlling factors. *Water Resources Research* 24, no. 7: 1011–1023.

Freund, R. 1965. A model of structural development of Israel and adjacent areas since Upper Cretaceous times. *Geological Magazine* 102, no. 3: 189–205.

Fridrich, C.J., W.W. Dudley, and J.S. Stuckless. 1994. Hydrogeological analysis of the saturated-zone ground water system, under Yucca Mountains, Nevada. *Journal of Hydrology* 154, no. 1–4: 133–168.

Gangi, A.F. 1978. Variation of whole and fractured porous rock permeability with confining pressure. *International Journal of Rock Mechanics and Mining Sciences & Geomechanics Abstracts* 15, no. 5: 249–257.

Ge, S., and S.C. Stover. 2000. Hydrodynamic response to strike- and dip-slip faulting in a half-space. *Journal of Geophysical Research B* 105, no. 1: 25,513–25,524.

Germanovich, L.N., and D.K. Astakhov. 2004. Fracture closure in extension and mechanical interaction of parallel joints. *Journal of Geophysical Research B* 109, no. 2: B02208, doi:10.1029/2002JB002131.

Guttman, J. 1980. Study of uranium isotopes in the Cenomanian-Turonian aquifer in the Yarqon-Taninim basin. M.Sc. thesis, Department of Geophysics, Tel Aviv University (in Hebrew).

Hamiel, Y., V. Lyakhovsky, and A. Agnon. 2005. Rock dilation, nonlinear deformation, and pore-pressure change under shear. *Earth and Planetary Science Letters* 237, no. 3–4: 577–589.

Hardy, S., and M. Ford. 1997. Numerical modeling of trishear fault propagation folding. *Tectonics* 16, no. 5: 841–854.

Harris, R.A. 1998. Introduction to special section: Stress triggers, stress shadows, and implications for seismic hazard. *Journal of Geophysical Research B* 103, no. 10: 24, 347–24, 358.

Hart, D.J., and H.F. Wang. 1999. Pore pressure and confining stress dependence of poroelastic linear compressibilities and Skempton's B coefficient for Berea sandstone. In *Rock Mechanics for Industry, Proceedings of the 37th U.S. Rock Mechanics Symposium, Balkema, Rotterdam*, ed. B. Amadei, R.L Kranz, G.A. Scott, and P.H. Smeallie, 365–371.

Hatzor, Y.H., and V. Palchik. 1997. The influence of grain size and porosity on crack initiation stress and critical flaw length in dolomites. *International Journal of Rock Mechanics and Mining Sciences & Geomechanics Abstracts* 34, no. 5: 805–816.

Hatzor, Y.H., M. Talesnik, and M. Tsesarsky. 2002. Continuous and discontinuous stability analysis of the bell-shaped caverns at Ben-Guvrin, Israel. *International Journal of Rock Mechanics and Mining Sciences & Geomechanics Abstracts* 39, no. 7: 867–886.

Hill, R. 1998. *The Mathematical Theory of Plasticity.* Oxford, U.K.: Oxford University Press.

Jaeger, J.C., and N.G.W. Cook. 1969. *Fundamentals of Rock Mechanics*. New York: Methuen.

Krenkel, E. 1924. Der Syrische Bogen. *Centralbl. Mineral*., 9, 274–281 and 10, 301–313.

Kwon, O., A.K. Kronenberg, A.F. Gangi, and B. Johnson. 2001. Permeability of Wilcox shale and its effective pressure law. *Journal of Geophysical Research B* 106, 19,339–19,353.

Lockner, D.A., and S.A. Stanchits. 2002. Undrained poroelastic response of sandstones to deviatoric stress change. *Journal of Geophysical Research B* 107, no. 12: 10.1029/2001JB001460.

Maimon, O., V. Lyakhovsky, A. Agnon, and M. Abelson. 2005. Stability of cavities and formation of sinkholes along the Dead Sea coast. Israel Geological Survey Report GSI/19/05. Jerusalem: Israel Geological Survey.

Mancy, K.H et al. 2000. Environmental protection of the shared Israeli-Palestinian mountain aquifer. Final report. A research project supported by USAID. Jerusalem and Bethlehem, Israel.

Mimran, Y. 1976. Deep-seated faulting and the structures of the northern Negev (Israel). An analytic and experimental study. *Israel Journal of Earth Sciences* 25, no. 3–4: 111–126.

Morrow, C.A., B.C. Zhang, and J.D. Byerlee. 1986. Effective pressure law for permeability of Westerly granite under cyclic load. *Journal of Geophysical Research B* 91, no. 3: 3870–3876.

Palchik, V., and Y.H. Hatzor. 2000. Correlation between mechanical strength and microstructural parameters of dolomites and limestones in the Judea Group-Israel. *Israel Journal of Earth Sciences* 49, no. 2: 65–79.

Paterson, M.S. 1978. *Experimental Rock Deformation—The Brittle Field*. Berlin, Germany: Springer-Verlag.

Poliakov A., Y. Podladchikov, E. Dawson, and C. Talbot 1996. Salt diapirism with simultaneous brittle faulting and viscous flow. In *Salt Tectonics, Geological Society Special Publication. Publ. No. 100*, ed. G.I. Alsop, D.J. Blundell, and I. Davison, 291–302. London, U.K.: Geological Society.

Poliakov, A., P. Cundall, Y. Podladchikov, and V. Lyakhovsky. 1993. An explicit inertial method for the simulation of viscoelastic flow: An evaluation of elastic effects on diapiric flow in two- and three-layer models. In *Proceedings of the NATO Advanced Study Institute on Dynamic Modeling and Flow in the Earth and Planets*, ed. K.E. Runcorn and D. Stone, 175–195. Dordrecht, The Netherlands: Kluwer.

Ramberg, H. 1981. *Gravity, Deformation and the Earth's Crust*, 2nd ed. London: Academic Press.

Raven, K.G., and J.E. Gale. 1985. Water flow in a natural rock fracture as a function of stress and sample size. *International Journal of Rock Mechanics and Mining Sciences & Geomechanics Abstracts* 22, no. 4: 251–261.

Reches, Z., D.F. Hoexter, and F. Hirsch. 1981. The structure of a monocline in the Syrian arc system, Middle East—Surface and subsurface analysis. *Journal of Petroleum Geology* 3, no. 4: 413–425.

Salvini, S., F. Storti, and K. McClay. 2001. Self-determining numerical modeling of compressional fault-bend folding. *Geology* 29, no. 9: 839–842.

Seaton, W.J., and T.J. Burbey. 2005. Influence of ancient thrust faults on the hydrogeology of the Blue Ridge Province. *Ground Water* 43, no. 3: 301–313.

Sibson, H.R. 1996. Structural permeability of fluid-driven fault-fracture meshes. *Journal of Structural Geology* 18, no. 8: 1031–1042.

Skempton, A.W. 1954. The pore-pressure coefficients A and B. *Geotechnique* 4, 143–147.

Suppe, J. 1985. *Principles of Structural Geology.* Englewood Cliffs, New Jersey: Prentice-Hall.

Suppe, J. 1983. Geometry and kinematics of fault-bend folding. *American Journal of Science* 283, no. 7: 684–721.

Turcotte, D.L., and G. Schubert. 1982. *Geodynamics, Applications of Continuum Physics to Geological Problems*. New York: John Wiley and Sons.

Vendeville, B.C. 2002. A new interpretation of Trusheim's classic model of salt-diapir growth. *Gulf Coast Association of Geological Societies Transactions* 52, 943–952.

Vendeville, B.C., and M.P.A. Jackson. 1992. The rise of diapirs during thin-skinned extension. *Marine and Petroleum Geology* 9, no. 4: 331–353.

Walsh, J.B. 1981. Effect of pore pressure and confining pressure on fracture permeability. *International Journal of Rock Mechanics and Mining Sciences & Geomechanics Abstracts* 18, no. 5: 429–435.

Walsh, J.B., and W.F. Brace. 1984. The effect of pressure on porosity and the transport properties of rock. *Journal of Geophysical Research B* 89, no. 11: 9425–9431.

Walsh, J.B., and M.A. Grosenbaugh. 1979. A new model for analyzing the effect of fractures on compressibility. *Journal of Geophysical Research B* 84, no. 7: 3532–3536.

Wang, H.F. 1997. Effects of deviatoric stress on undrained pore pressure response to fault slip. *Journal of Geophysical Research B* 102, no. 8: 17,943–17,950.

Weijermars R., M.P.A. Jackson, and B.C. Vendeville. 1993. Rheological and tectonic modeling of salt provinces. *Tectonophysics* 217, no. 1–2: 143–174.

Weismayr, G., and B., Grasemann. 2005. Sense non-sense of shear in flanking structures with layer-parallel shortening: Implications for fault-related folds *Journal of Structural Geology* 27, 249–264.

Wirt, L., and H.W. Hjalmarson. 1999. Sources of springs supplying base flow to the Verde River headwaters, Yavapai County, Arizona. USGS Open-File Report 99-0378. Reston, Virginia: USGS.

Yechieli, Y., U. Kafri, M. Goldman, and C.I. Voss. 2001. Factors controlling the configuration of the fresh-saline water interface in the Dead Sea coastal aquifers: Synthesis of TDEM survey and numerical ground water modeling. *Hydrologic Journal* 9, no. 4: 367–377.